Universal formation dynamics and noise of Kerr-frequency combs in microresonators

T. Herr[1], K. Hartinger[1,2], J. Riemensberger[1], C. Y. Wang[1,3], E. Gavartin[1], R. Holzwarth[2,3], M. L. Gorodetsky[4] and T. J. Kippenberg[1,3]*

Optical frequency combs allow for the precise measurement of optical frequencies and are used in a growing number of applications. The new class of Kerr-frequency comb sources, based on parametric frequency conversion in optical microresonators, can complement conventional systems in applications requiring high repetition rates such as direct comb spectroscopy, spectrometer calibration, arbitrary optical waveform generation and advanced telecommunications. However, a severe limitation in experiments working towards practical systems is phase noise, observed in the form of linewidth broadening, multiple repetition-rate beat notes and loss of temporal coherence. These phenomena are not explained by the current theory of Kerr comb formation, yet understanding this is crucial to the maturation of Kerr comb technology. Here, based on observations in crystalline MgF_2 and planar Si_3N_4 microresonators, we reveal the universal, platform-independent dynamics of Kerr comb formation, allowing the explanation of a wide range of phenomena not previously understood, as well as identifying the condition for, and transition to, low-phase-noise performance.

Optical frequency combs[1–4] have revolutionized the field of frequency metrology and spectroscopy and are enabling components in a range of applications[5]. Recently, a novel class of frequency comb generators has been discovered[6] by coupling a continuous-wave (c.w.) laser to a high-finesse fused silica microcavity, where the Kerr nonlinearity enables (cascaded) four-wave-mixing (FWM), resulting in an optical frequency comb. These Kerr combs could complement conventional frequency combs in applications where high power per comb line (typically >100 μW) and high repetition rate (>10 GHz spacing between the comb lines) are desirable[7], such as in astronomical spectrometer calibration[8–10], direct comb spectroscopy[11], arbitrary optical waveform generation[12,13] and advanced telecommunications. The creation of Kerr combs using microresonators has been demonstrated in crystalline CaF_2 (refs 14,15) and MgF_2 (refs 16–18) resonators, fused-silica microspheres[19], planar high-index silica[20] and Si_3N_4 ring resonators[21,22], and compact fibre cavities[23]. Over recent years, a significant advance in Kerr comb technology has been achieved by demonstrating a single and well-defined radio-frequency (RF) beat note between adjacent comb lines (corresponding to the equidistant comb spacing and required for stabilizing the comb)[6,14,24], a fully phase-stabilized Kerr comb[24], the generation of octave-spanning spectra (required for self-referencing the comb using the f–$2f$ scheme)[25,26], the detection and shaping of pulses[13], and extension of spectral coverage towards the visible[27] and mid-infrared spectral regimes[18]. In addition to these experimental advances, theoretical work[28,29] has also enabled an explanation of the power distribution of Kerr combs, particularly the first comb modes appearing not necessarily adjacent to the pump. Despite these advances, however, recent work aiming at broader spectra and lower repetition rates (as required for practical applications), reported linewidth broadening in octave-spanning spectra[25] and multiple RF beat notes in low-repetition-rate[30] fused-silica Kerr comb systems. Moreover, recent complementary studies in the time domain have revealed distinct paths to comb formation

resulting in either highly or partially coherent behaviour[13]. Understanding the underlying processes responsible for these phenomena is not only an as-yet unresolved scientific question, but is indeed crucial for bringing this new technology to maturity[7].

In this Article, we describe the origin of these phenomena, attributing this to a universal platform-independent behaviour in Kerr comb generators. We present guidelines for the design of Kerr comb generators and, based on theoretical analysis and experimental observation, derive the condition under which narrow and well-defined beat notes are obtained. The presented understanding also explains the low-frequency amplitude noise observable in Kerr combs.

Experimental systems

We used two entirely different experimental systems—crystalline MgF_2 resonators[16–18] and Si_3N_4 microring resonators[21] (typical resonance widths of $\kappa/2\pi \approx 1$ MHz and 200 MHz, respectively)—for Kerr comb generation (Fig. 1d). The comb emerges when the thermally locked[31] blue-detuned pump laser, which is evanescently coupled to the resonator (via a tapered fibre or a planar waveguide, close to critical coupling), is tuned into resonance, thereby increasing the circulating power inside the resonator. The resonators were pumped using narrow-linewidth fibre and diode lasers (<100 kHz, <300 kHz short term) and amplified by an erbium-doped fibre amplifier. Parametric frequency conversion set in once the parametric threshold[32] was reached. As in previous work in fused-silica microresonators[25], a broad RF beat note was observed in both systems (Fig. 1a,b).

Multiple and broad RF beat notes

A multitude of physical processes can account for or contribute to the observation of broad RF beat notes. These include line-broadening phase-noise mechanisms such as thermorefractive noise, thermoelastic noise, thermal Brownian motion, ponderomotive noise, photothermal noise, laser phase noise and self-/cross-phase
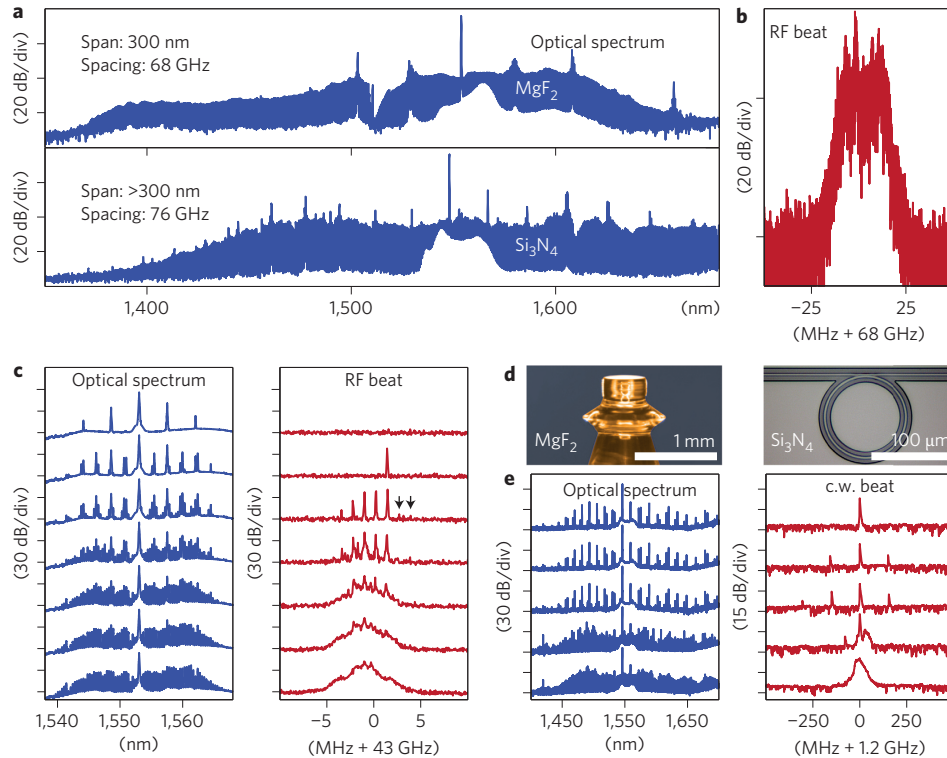
Figure 1 | Multiple and broad beat notes. a, Optical frequency comb generation in crystalline MgF_2 (pump power = 500 mW) and Si_3N_4 (pump power = 3 W) microresonators. **b**, Both spectra exhibit broad RF beat notes, shown here for the MgF_2 spectrum (resolution bandwidth RBW = 300 kHz). **c**, Evolution of the optical frequency comb spectrum (blue, pump power = 50 mW) and RF beat note (red, RBW = 100 kHz) generated in a 43 GHz FSR MgF_2 resonator while tuning the pump laser into resonance. Arrows indicate smaller peaks. **d**, Optical images of typical crystalline MgF_2 and planar Si_3N_4 resonators. **e**, As in **c** but for a 200 GHz FSR Si_3N_4 ring resonator (pump power = 3 W). The measurement of the RF beat note is replaced by an equivalent beat note measurement between a comb line and an external continuous-wave (c.w.) laser.

modulation[25,33–35]. Phase noise can also be generated by optomechanical coupling[36–38] of optical and mechanical resonator modes, by thermal oscillations of the resonator[39], as well as by the interaction of light with different transverse modes[27].

To shed light on the origin of the broad RF beat note, we investigated the beat note at different stages during comb formation. Figure 1c,e reveals an intriguing behaviour in both systems. The broad beat note, visible in the lowermost data set, consists of a discrete spectrum of multiple narrow beat notes, the number of which increases as more power is coupled to the resonator. It is often observed that both the intensity and frequency of these beat notes can change continuously or discontinuously when the laser detuning is varied. This result unifies the observations of broad and multiple beat notes made individually in earlier work[25,30]. The phenomenology prevails both in the crystalline MgF_2 and Si_3N_4 systems, despite their vastly different geometries and material characteristics, thereby showing the universality of the phenomenon. By interpreting broad and multiple beat notes as identical phenomena, pure line-broadening phase-noise mechanisms (such as those mentioned above) can be excluded as the principal cause of the observations (Supplementary Section I).

Although, recently, there have been reports of frequency combs on transverse order modes in crystalline resonators[27], these multimode effects are unlikely to account for the observations. The results of broadband resonator spectroscopy (as in ref. 40) show that, except for (avoided) mode crossings, the resonances are generally separated by several gigahertz in Si_3N_4. Interaction via FWM between different mode families (with generally different free spectral ranges, FSRs) is suppressed by the requirement for conservation of angular momentum[32]. Although crystalline resonators support mechanical radial breathing modes[41] as well as surface acoustic modes[38,42],

which could equally give rise to multiple modulation beat notes and chaotic optomechanical oscillations[43], the on-chip encapsulated geometry of the Si_3N_4 system (which has no free boundaries due to the embedding oxide) renders mechanical oscillations implausible. Instead, we suggest that the cause for the broad and multiple beat notes lies in the dynamics of Kerr comb formation itself.

Kerr comb formation

Figure 2a explains schematically the initial states of Kerr comb formation. The first comb lines are generated in a degenerate FWM process, symmetrically to the pump frequency ω_p, as soon as the parametric gain overcomes the loss of the cavity (Fig. 2a, state 1). The distance (in terms of relative mode number μ) of the new lines to the pump depends on the pump power and the dispersion of the resonator. The latter determines the cold resonance frequencies through

$$\omega_\mu = \omega_0 + D_1 \cdot \mu + \frac{1}{2} D_2 \cdot \mu^2 + \cdots$$

where ω_0 is the resonance frequency of the pumped mode, $D_1/2\pi$ corresponds to the FSR of the resonator and $D_2/2\pi$ to the difference of the two FSRs adjacent to the expansion frequency ω_0 (Fig. 2c). Note that D_2 is linked to the group velocity dispersion through the relation $D_2 = -c/n_0 \cdot D_1^2 \cdot \beta_2$ (ref. 27), where n_0 is the refractive index and c the speed of light. It has been observed that the first lines can oscillate either in the resonator mode directly adjacent to the pump or at a multiple of this distance[13,20,44–46]. This can be understood within the framework of nonlinear coupled mode equations[28,29] as detailed below and in Supplementary Section II. In simple terms, the sidebands are generated where the
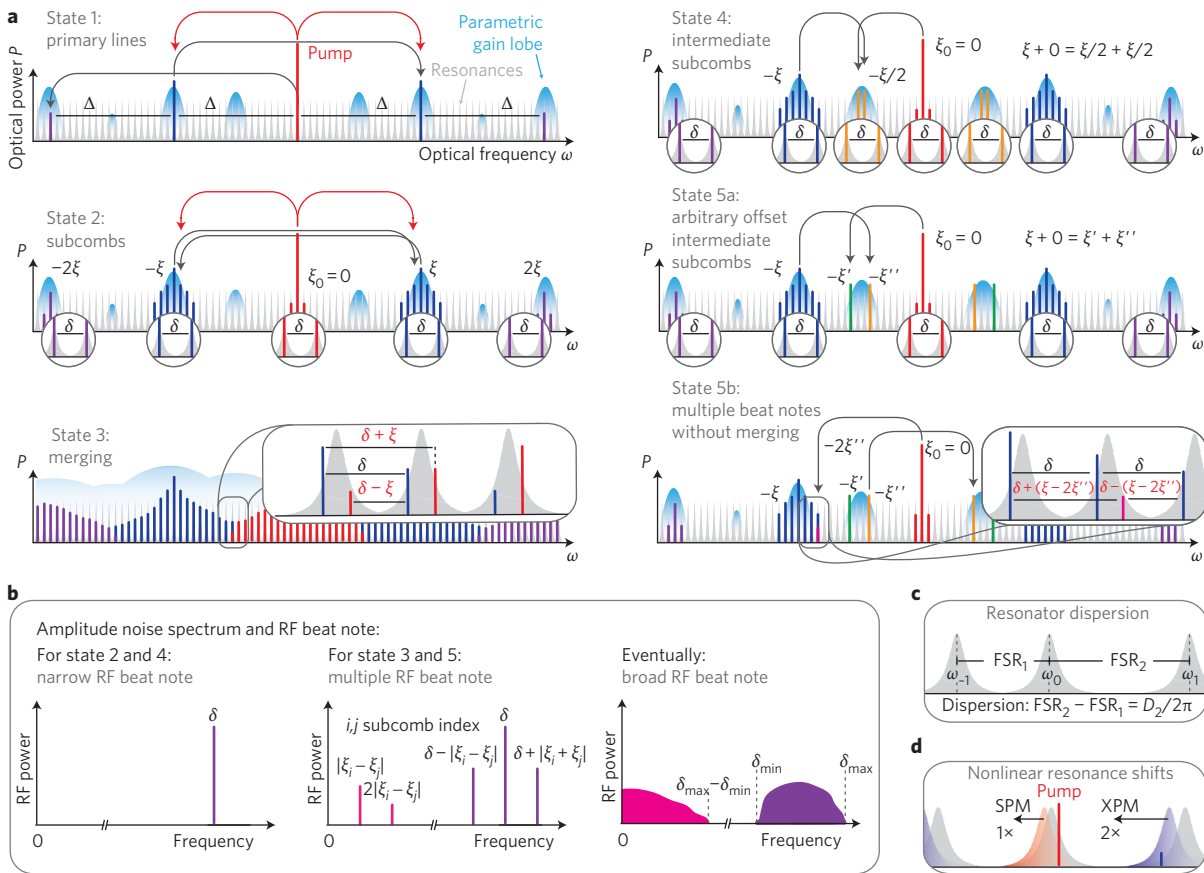
Figure 2 | Kerr comb formation. a, State 1: generation of primary sidebands (spaced by Δ) via FWM. State 2: secondary lines generated around the primary lines form subcombs with a native spacing δ. The spacing Δ is not generally an integer multiple of δ; that is, the subcombs have different offset frequencies $0, \pm\xi, \pm2\xi\ldots$ State 3: the subcombs merge into a gap-free spectrum (multiple lines can exist in a single resonance). Consequently, multiple RF beat notes (see **b**) appear. State 4: natively spaced secondary comb lines may also emerge between primary lines at an averaged offset frequency. State 5a: non-natively spaced secondary comb lines may be generated between primary lines with arbitrary offsets. State 5b: as a result of state 5a, multiple RF beat notes can appear before the spectral gaps are closed (see **b**). **b**, Single, multiple and broadband electronic signals present in the Kerr comb spectrum. **c**, Resonator dispersion D_2. **d**, Self- and cross-phase modulation (SPM, XPM) by the pump on the pumped resonance (red) and other cavity resonances (blue). The frequency shift caused by XPM is twice the shift caused by SPM.

dispersion D_2, nonlinear mode shifts (via self- and cross-phase modulation) and pump laser detuning compensate one another (Fig. 2d).

In the following, we distinguish two scenarios of comb formation and refer to these scenarios as multiple mode-spaced (MMS) and natively mode-spaced (NMS) combs. In MMS combs the first parametric sidebands are generated at a spacing Δ (corresponding to a multiple mode number difference, $|\mu| > 1$) away from the pump (Fig. 2a, Supplementary Section II). Cascaded FWM transfers the initial spacing Δ to higher-order sidebands. The initial spacing Δ is preserved and reproduced between all emerging lines due to the conservation of energy in parametric processes[6]. We refer to these initial sidebands spaced by Δ as primary comb lines. At a later stage of comb evolution (that is, reduced detuning and increased circulating power), secondary lines are generated around the primary lines via degenerate or non-degenerate FWM processes (Fig. 2a, state 2 and Supplementary Section III), resulting in natively δ-spaced lines in neighbouring resonator modes ($\delta/2\pi \approx$ FSR). The formation of lines in a second degenerate process can be understood in terms of parametric gain lobes that are broad enough to allow neighbouring modes to be populated. The spectrally separated subcombs initiated in these processes grow through non-degenerate FWM when the power coupled to the cavity is increased further, and eventually merge to form a gap-free spectrum of lines

(Fig. 2a, state 3). The non-degenerate process may also yield lines between two previously existing strong lines (Fig. 2a, states 4 and 5a). Combs of the MMS type with this spectral evolution have so far been observed in systems with a smaller FSR (10–100 GHz) or high pump power ($\gtrsim 1$ W)[13,20,25,44,46].

In NMS combs the first parametric sidebands are generated in the modes $\mu = +1, -1$ adjacent to the pump[6,32]. As such NMS combs are a special case of MMS combs where $\Delta = \delta$, and non-degenerate cascaded FWM leads to the generation of a frequency comb spectrum growing outwards from the pump. In reverse, MMS combs can be interpreted as NMS but with correspondingly higher FSR as long as only the primary lines exist.

In the following, we will investigate the properties of MMS combs to understand if and how their formation mechanism affects the width and number of RF beat notes. To do so, we perform a multi-heterodyne experiment for a Kerr comb generated in a MgF_2 resonator with an FSR of 35 GHz and a conventional stabilized mode-locked fibre laser comb with a 250 MHz repetition rate. As detailed in the Methods ('Multi-heterodyne experiment'), this allows an accurate determination of the spacing between select Kerr comb lines (Fig. 3). Here, we address the vital question of the commensurability of the primary and secondary comb lines (Fig. 3a,b). More precisely, we test whether the primary spacing Δ is an integer multiple of the native spacing δ, that is, whether the
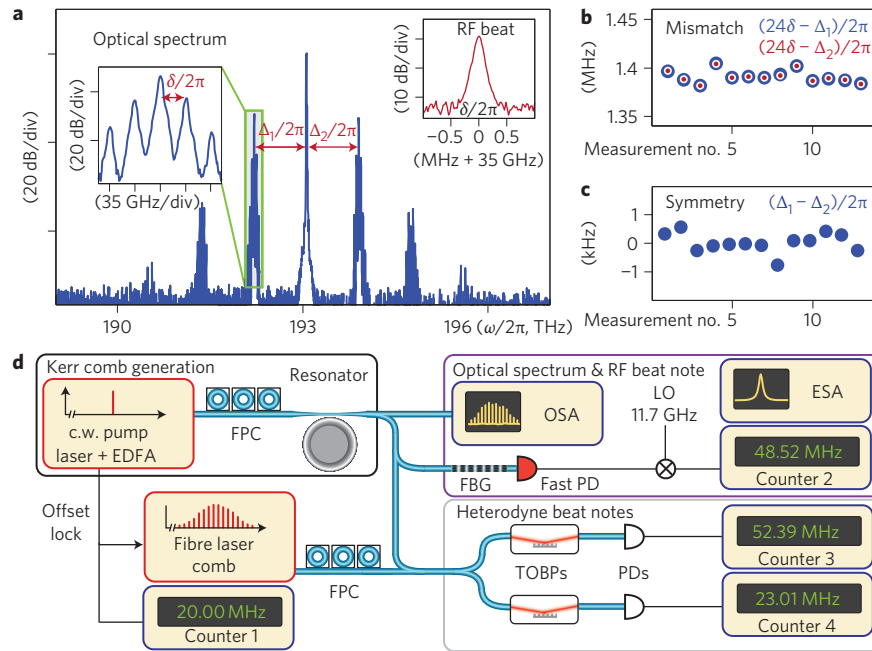
Figure 3 | Commensurability of subcombs. a, Optical Kerr comb spectrum generated in a 35 GHz FSR MgF_2 resonator (pump power = 80 mW, pump laser offset-locked to a fibre laser comb, primary spacing Δ corresponds to 24 FSRs). The secondary comb lines around the primary lines are spaced by the native spacing δ. The resulting RF beat note consists of a single and narrow signal (see right inset, 35 dB in a resolution bandwidth of 300 kHz). Heterodyne beat notes are generated between the innermost primary Kerr comb lines and a conventional 250 MHz fibre laser comb. Frequency counting of all beat notes allows for a precise determination of the frequency distances δ, Δ_1 and Δ_2. **b**, The spacings Δ_1 and Δ_2 are not integer multiples of δ, but show a mismatch of $2\pi \cdot 1.4$ MHz. **c**, Difference between Δ_1 and Δ_2 as indicated in **a**. No deviation is detected from the symmetry of the primary comb lines with respect to the pump. **d**, Experimental set-up. EDFA, erbium-doped fibre amplifier; FPC, fibre polarization controller; OSA, optical spectrum analyser; ESA, electronic spectrum analyser; FBG, fibre Bragg grating (attenuates the pump by 30 dB); LO, local oscillator; PD, photodiode; TOBP, tunable optical bandpass filter.

generated optical spectrum forms an intermittent but consistent frequency comb, the gaps of which can be filled by increasing the coupled power and extending the existing subcombs. Strikingly, we find that this is not the case. A mismatch of $(\mu \cdot \delta - \Delta)/2\pi \approx$ 1.4 MHz ($\mu = 24$) between the actual and expected positions of the primary comb line is observed, assuming a comb line grid with spacing δ centred on the pump laser frequency. This mismatch exceeds the precision of the measurement by far. The redundancy in performing this measurement with a pair of symmetric primary comb lines rules out artefacts in the frequency counting such as cycle slips that would lead to an incorrectly detected mismatch. Importantly, the RF beat note resulting from mutual beating between neighbouring natively δ-spaced comb lines is found to be well-defined and unique over the full spectral width of the comb spectrum (Fig. 3a, right inset). Based on these observations, we conclude that the optical spectrum consists of multiple equidistant combs of index i, composed of lines of index n, at optical frequencies $\omega_n^{(i)}$ separated by the same spacing δ:

$$\omega_n^{(i)} = \omega_p + \xi_i + n \cdot \delta, \quad n = 0, \pm 1, \pm 2, \dots$$

These equidistant combs have non-commensurate offset frequencies $\xi_j \neq \xi_i + n \cdot \delta$, $j \neq i$, as illustrated in Fig. 2a, state 2. Whenever isolated lines (that is, not in the direct vicinity of existing lines) are generated (Fig. 2a, states 4 and 5a), new subcombs with new offsets are defined, which then grow as described above. While the process shown in Fig. 2a, state 5a, results in arbitrarily offset subcombs, processes similar to state 4 result in a set of subcombs with equal relative offset difference $\Delta\xi$ to their respective nearest-neighbour subcomb as observed experimentally in Figs 4c,5b.

Even though all subcombs are spectrally separated and reside at spectral positions with different resonator FSRs, their individual spacings δ are equal, resulting in a single narrow overall RF beat note (Fig. 2b). This observation becomes clear when switching from a frequency- to a time-domain picture. FWM can then be interpreted as a time-dependent modulation of the effective refractive index of the resonator, affecting all modes equally (assuming similar mode profiles). Once generated, the spacing δ is therefore transferred to all spectral locations of the comb.

A critical point is reached when the growth in bandwidth of the subcombs closes their spectral separation and leads to an overlap (Fig. 2a, state 3). As the combs begin to merge, individual resonator modes are populated by multiple lines with slightly different optical frequencies. When monitoring the RF beat note on an electronic spectrum analyser (ESA), sidebands appear around δ, with frequencies $\delta_\pm^i = \delta \pm \Delta\xi_i$ and $\Delta\xi_i = \xi_{i+1} - \xi_i$ (this being the offset difference between the two merging combs). This can be seen schematically in Fig. 2b or experimentally in Fig. 1c (third data set from the top). Once these new RF beat notes are generated, they can spread throughout the optical comb spectrum, effectively leading to multiple lines within individual resonator modes and correspondingly even more RF beat notes $\delta_\pm^{i,j} = \delta \pm \Delta\xi_{i,j}$ and $\Delta\xi_{i,j} = \xi_i - \xi_j$. Eventually, this results in a broad RF beat note as indicated in Fig. 2b. We emphasize that the emergence of phase noise is not a consequence of large spectral width. Note that not all possible side beat notes $\delta_\pm^{i,j} = \delta \pm \Delta\xi_{i,j}$ may be generated, as the finite cavity bandwidth will suppress lines far off the resonance frequencies. Also, multiple beat notes can be observed even before the spectral gaps close when FWM processes similar to those in Fig. 2a (states 5a and b), occur (Supplementary Section IV). The described pathways to multiple and broad RF beat notes are
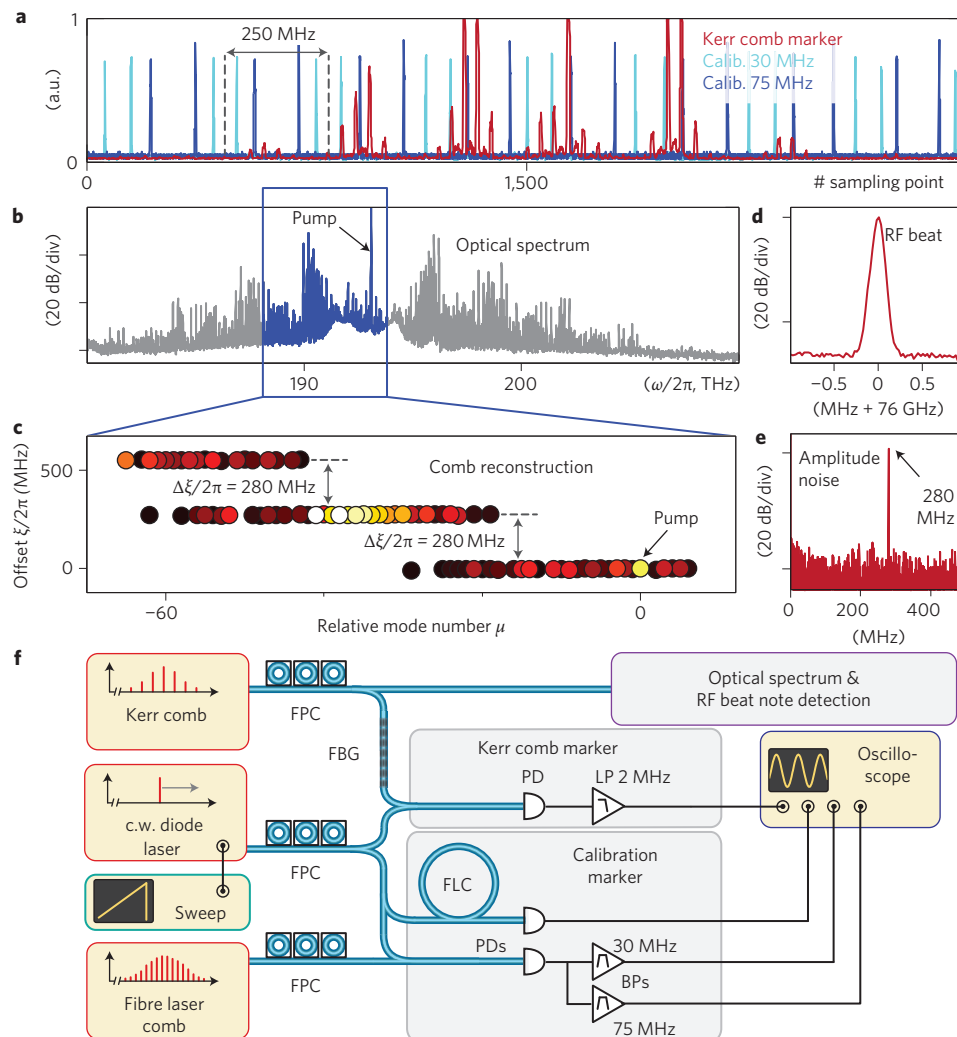
Figure 4 | Kerr comb reconstruction. a, Fraction of raw data showing frequency calibration (light and dark blue) and Kerr comb marker (red); for details see Methods. Data correspond to a 2 GHz wide scan resolving multiple comb lines generated in a single resonance of a 76 GHz FSR Si_3N_4 resonator (pump power = 5 W). **b**, Optical spectrum of another Kerr comb (as in **a** but with different detuning). The blue 6 THz wide section corresponds to the scanned reconstruction range. **c**, Visualization of the reconstructed Kerr comb showing the offsets ξ of the comb lines versus their relative mode numbers μ (lighter colours correspond to higher comb line power). Three subcombs are visible, with relative offsets of $\Delta\xi/2\pi = 280$ MHz. **d**, RF beat note of the comb in **b** (resolution bandwidth RBW = 100 kHz) corresponding to δ. **e**, Amplitude noise spectrum with a peak at 280 MHz resulting from the beating between the offset subcombs (RBW = 100 kHz). **f**, Set-up for Kerr comb reconstruction. FLC, fibre loop cavity; LP/BP, low-/bandpass filter. Other abbreviations as in Fig. 3d.

absent in NMS combs, which is in agreement with previous experimental observation[6,18].

This hypothesis can also explain a further previously unexplained phenomenon observed in MMS combs (in a state corresponding to state 3 or 5b in Fig. 2a). If the electronic spectrum of the transmitted light is recorded, amplitude noise features (that is, with Fourier frequency $\Omega \ll \delta$) appear, the emergence of which coincides with the generation of the frequency comb (Fig 2b, Supplementary Section V). Indeed, although the spacings δ, $\delta_{\pm}^{i}$ and $\delta_{\pm}^{i,j}$ are close to the FSR of the resonator and therefore require dedicated RF equipment for their detection, this phenomenon finds its equivalent in the lower RF regime, where the frequencies $\Delta\xi_i$ and $\Delta\xi_{i,j}$ can readily be measured at a much lower frequency in the comb spectrum. In particular, broad RF beat notes at frequencies corresponding to the native spacing will coexist with a broad signal at low frequencies close to d.c. This provides sensitive and easy access to noise analysis of Kerr combs.

To support the presented hypothesis further, we performed a broadband spectroscopic reconstruction of the generated comb with close to megahertz resolution over a range of ∼6 THz (Fig. 4). This novel method enabled a line-by-line reconstruction of the Kerr comb, that is, a measurement of the frequency differences between a large number of comb lines. The experimental set-up is shown in Fig. 4f (for details see Methods, 'Kerr comb reconstruction'). As an example, a fraction of raw data showing that more than one comb line can exist in a single cavity resonance is shown in Fig. 4a. This behaviour is surprising and not contained in the present understanding of Kerr combs. Moreover the comb reconstruction reveals individual subcombs with different offset frequencies ξ, but identical comb line spacing. This latter characteristic is further evidenced by the narrow and well-defined RF beat note shown in Fig. 4d. Note that multiple beat notes are not observed in this case, as the overlap between the individual subcombs is too small and the signal is dominated by the more powerful subcomb centres. The amplitude noise, however, provides a more sensitive method capable of detecting the beating between the slightly overlapping subcombs (Fig. 4e).
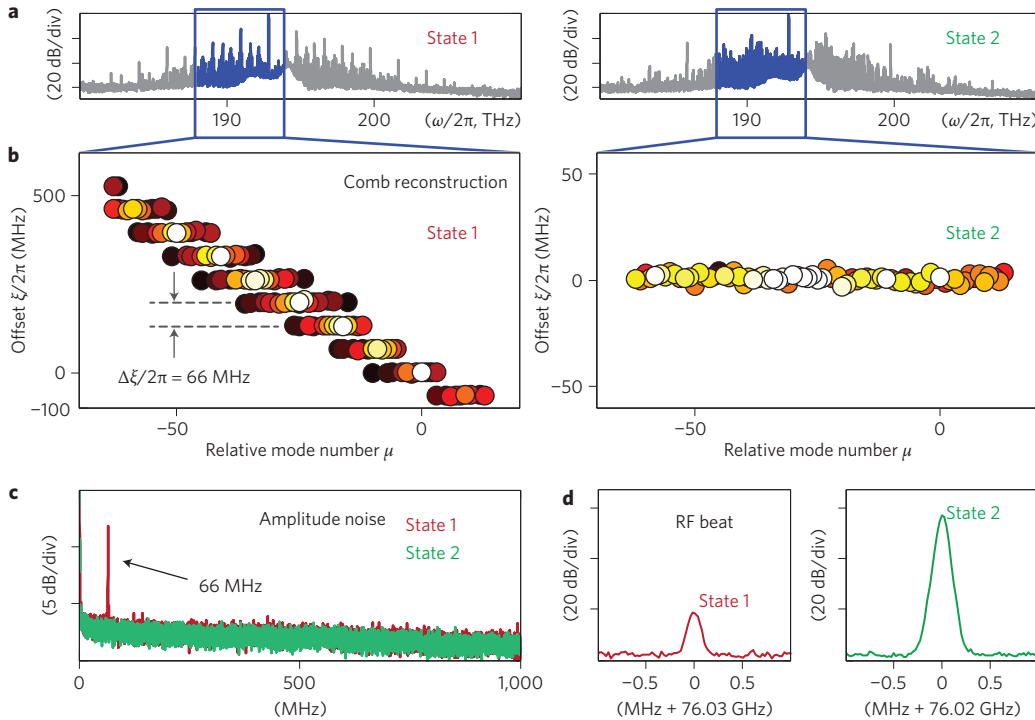
Figure 5 | Transition to a low phase noise Kerr comb. a, Optical spectra of two microresonator comb states 1 and 2 (pump power = 6 W) in a Si_3N_4 resonator. State 2 evolves from state 1 when reducing the detuning of the pump laser. **b**, A transition is observed from multiple subcombs to a single (sub)comb over the bandwidth of the Kerr comb reconstruction. In state 1, all subcombs have the same mode spacing, but have different offsets ξ, which differ by a constant relative amount of $\Delta\xi/2\pi = 66$ MHz. **c**, In the transition from state 1 to state 2, the amplitude noise peak resulting from the beating between overlapping offset subcombs disappears (resolution bandwidth RBW = 300 kHz) **d**, The RF beat note shifts by ≈ 10 MHz and the signal-to-noise ratio increases (RBW = 100 kHz).

In a second comb reconstruction experiment we observed a transition from a spectrum composed of multiple and offset subcombs to one that exhibited only a single (sub)comb over the full reconstruction range (Fig. 5) when reducing the pump laser detuning (which affects the subcomb offsets and the comb line spacing). The fact that the amplitude noise vanishes suggests that the full spectrum forms a consistent frequency comb. This observation could explain a similar behaviour in amplitude noise observed very recently in a Si_3N_4 system[26]. The detected RF beat note for both comb states is well-defined and narrow, but the signal-to-noise ratio increases from 20 dB to almost 60 dB in the second state. We attribute this transition to a δ–Δ-matching where commensurability between the spacings δ and Δ is achieved by appropriate choice of laser power and detuning, which affect comb offset and spacing in a distinct manner[26]. Note that a similar transition could not be achieved for the comb in Fig. 4. Reducing the laser detuning results in the reappearance of amplitude noise peaks and eventually broadband amplitude noise and a broad RF beat note.

Role of dispersion and resonance width

In the following, we show that the ratio κ/D_2 of resonance width to dispersion (at the pump wavelength) is closely linked to whether a comb evolves along the NMS or MMS pathways, thereby affecting the RF beat note. To estimate under which conditions NMS combs can be achieved, we determine the distance in terms of mode number between pump and first sideband (similar to previous work, such as refs 28, 29, 32, 45 and 47) by solving the nonlinear coupled mode equations and deriving the parametric gain for the initial degenerate FWM process, where we include the detuning of the pump laser as well as the detuning of the generated sidebands with respect to the cavity resonances. For a constant launched pump power P_{in} and tuning the pump laser into resonance from

the higher frequency side, the circulating power inside the cavity increases. The first sidebands with mode numbers $\pm\mu_{th}$ are generated when the parametric threshold is reached, that is, when the gain overcomes the cavity decay rate κ (for details, see Supplementary Section II):

$$\mu_{th} \simeq \sqrt{\frac{\kappa}{D_2}\left(\sqrt{\frac{8\eta P_{in}cn_2\omega_p}{\kappa^2 n_0^2 V_{eff}}-1}+1\right)}$$

where η denotes the coupling strength ($\eta = 1/2$ for critical coupling), ω_p is the pump frequency, n_2 is the nonlinear index, and V_{eff} is the effective nonlinear mode volume.

The primary mode spacing observed for the 35 GHz FSR MgF_2 resonator in Fig. 3a ($\eta = 0.5$, $\omega_p/2\pi = 193$ THz, $n_2 = 0.9 \times 10^{-20}$ m^2 W^{-1}, $n_0 = 1.37$, $V_{eff} = 6.2 \times 10^{-13}$ m^3, $\kappa/2\pi = 1$ MHz, $P_{in} = 0.1$ W) corresponds to a dispersion of $D_2/2\pi = 11$ kHz, which is consistent with the measured dispersion (following ref. 40) of $D_2/2\pi \approx 10$ kHz.

The smallest possible $\mu_{th,min}$ is achieved if the threshold is reached with the pump laser exactly resonant with the cavity. This can be achieved approximately by carefully setting the pump power P_{in} or by applying injection locking to the pump laser[48]. In this ideal case the previous equation simplifies to

$$\mu_{th,min} = \sqrt{\frac{\kappa}{D_2}}$$

The above derivation assumes that D_2 dominates over higher-order dispersion terms. This is not the case in the direct vicinity of the zero dispersion point, where a similar analysis following the one above, but including higher-order terms, is required.

Discussion and conclusion

Our experimental observations and theoretical analysis fully explain the observation of broad[25] and multiple beat notes[30], amplitude noise, sudden drops of this noise for certain comb states[26], and loss of coherence in time-domain experiments[13]. In addition, our study identifies $\sqrt{(\kappa/D_2)}$ as the important figure of merit for the design of low-phase-noise Kerr comb generators (where $D_2 > 0$ describes anomalous dispersion). For intrinsically low-noise Kerr combs (that is, emerging symmetrically in steps corresponding to single FSRs around the pump laser) the ratio κ/D_2 should be close to unity. This can be achieved by reducing the cavity decay rate or by increasing the anomalous dispersion. Note that $\sqrt{(\kappa/D_2)} \approx 1$ has previously been achieved, for example, in ref. 6. We also note that the condition $\mu_{th} \approx 1$ is not a strict one and a detuning-dependent transition from multiple subcombs to a broadband, single comb (Fig. 5) can occur, which we attribute to a δ–Δ-matching. Many systems, such as Si_3N_4 resonators, allow for great freedom in their design parameters, enabling geometries with strongly anomalous dispersion. The dispersion D_2 also depends on the pump wavelength. This is particularly important for the mid-infrared regime where low-noise Kerr comb generation has been demonstrated recently in the strong anomalous dispersion regime at 2.5 μm (ref. 18). Another way of influencing dispersion D_2 is to increase the FSR of the resonator, as D_2 can be interpreted as the material and geometrical dispersion of the resonator integrated over the frequency interval of one FSR. This explains why systems with large FSR are advantageous in generating NMS combs. The specific use of avoided modal crossings in resonators[49,50] may provide an elegant way of achieving locally strongly anomalous dispersion at the pump wavelength (while retaining an elsewhere moderate dispersion facilitating broadband Kerr comb generation), resulting in narrowly spaced primary sidebands and low-phase-noise combs.

Methods

Multi-heterodyne experiment. A narrow-linewidth, 1,553 nm continuous-wave fibre laser was amplified using an erbium-doped fibre amplifier (amplified spontaneous emission filtered) to a power of 80 mW and sent to the MgF_2 resonator for Kerr comb generation. The pump laser was offset-locked to 20 MHz below a line of a fibre laser comb with a repetition rate of 250 MHz. The performance of the lock was verified by a RF counter. The resonator was thermally locked to the pump laser and the system given sufficient time to thermalize before each measurement. After comb generation the generated spectrum was split into several beams. One beam was sent to an optical spectrum analyser for detection of the optical Kerr comb spectrum, and a second to a fast photodiode (bandwidth, 45 GHz) for detection of the RF beat note between natively spaced neighbouring comb lines. The electronic signal generated in the fast photodiode was down-mixed using the third harmonic of an RF generator at 11.7 GHz and sent to an electronic spectrum analyser and another frequency counter. Note that the pump was attenuated by ~30 dB using a narrow (only affecting the pump laser line) fibre Bragg grating in transmission. Finally, two more beams were combined with the spectrum of the fibre laser comb. Two tunable optical bandpass filters (bandwidth, 0.8 nm) were used to filter out a narrow spectral region of the combined comb spectra at the position of the primary comb lines and sent to two photodiodes for detection of the heterodyne beat note between the two combs (typically with a signal-to-noise ratio exceeding 20 dB in a resolution bandwidth of 300 kHz). The beat note frequencies were determined by frequency counters with a gate time of 0.1 s. The heterodyne beat notes, in combination with the offset lock of the pump, allowed the accurate determination of the frequency difference between the primary comb lines and the pump laser. We have assumed that the Kerr comb lines do not deviate by more than 250 MHz from their expected positions based on the FSR of the resonator.

Kerr comb reconstruction. The set-up follows the approach introduced in ref. 40 and is developed further to reconstruct spectrally the Kerr comb spectra. To this end, a diode laser, scanning over a frequency interval of ~6 THz (from 1,545 nm towards longer wavelengths) is split into three beams, two of which are used for frequency calibration of the laser scan. The first calibration beam is combined with the spectrum of a fibre laser comb with a repetition rate of 250 MHz. The signal is detected by a photodiode and the resulting RF signal is bandpass-filtered around 30 and 75 MHz with a bandwidth of 1 MHz, and continuously recorded by an oscilloscope during the scan (10 Msamples, peak-detect mode). Whenever the scanning laser sweeps over a position 30 MHz or 75 MHz below or above the fibre laser comb line, a RF signal passes the bandpass filter, resulting in four calibration markers per comb line in the oscilloscope traces. Based on these, the instant in time when the laser crosses a fibre laser comb line can be found. This allows the definition of a relative detuning of the pump laser as a function of time during the scan. To rule out artefacts in the scan (such as mode hops that could mimic offsets between subcombs), the consistency of the 30 and 75 MHz markers were verified. In addition, a second calibration beam from the diode laser is coupled to a fibre-loop cavity (FLC) with a FSR of ~10 MHz, and the transmission is recorded simultaneously on another oscilloscope channel. The consistency of this signal with the calibration obtained from the fibre laser comb markers is verified and limits the effect of scan artefacts to below a few megahertz. The third diode laser beam is used to probe the Kerr comb spectrum by generating and recording RF markers. Here, we used a 1.9 MHz low-pass filter, which directly maps the Kerr comb, line by line, onto the frequency-calibrated scan trace. The main limitation in the measurement comes from the jitter of the pump and scan diode lasers.

References

1. Holzwarth, R. *et al.* Optical frequency synthesizer for precision spectroscopy. *Phys. Rev. Lett.* **85,** 2264–2267 (2000).
2. Jones, D. J. *et al.* Carrier-envelope phase control of femtosecond mode-locked lasers and direct optical frequency synthesis. *Science* **288,** 635–639 (2000).
3. Udem, T., Holzwarth, R. & Hänsch, T. W. Optical frequency metrology. *Nature* **416,** 233–237 (2002).
4. Cundiff, S. T. & Ye, J. Colloquium: femtosecond optical frequency combs. *Rev. Mod. Phys.* **75,** 325–342 (2003).
5. Newbury, N. R. Searching for applications with a fine-tooth comb. *Nature Photon.* **5,** 186–188 (2011).
6. Del'Haye, P. *et al.* Optical frequency comb generation from a monolithic microresonator. *Nature* **450,** 1214–1217 (2007).
7. Kippenberg, T. J., Holzwarth, R. & Diddams, S. A. Microresonator-based optical frequency combs. *Science* **332,** 555–559 (2011).
8. Murphy, M. T. *et al.* High-precision wavelength calibration of astronomical spectrographs with laser frequency combs. *Mon. Not. R. Astron. Soc.* **380,** 839–847 (2007).
9. Steinmetz, T. *et al.* Laser frequency combs for astronomical observations. *Science* **321,** 1335–1337 (2008).
10. Li, C. H. *et al.* A laser frequency comb that enables radial velocity measurements with a precision of 1 cm s^{-1}. *Nature* **452,** 610–612 (2008).
11. Diddams, S. A., Hollberg, L. & Mbele, V. Molecular fingerprinting with the resolved modes of a femtosecond laser frequency comb. *Nature* **445,** 627–630 (2007).
12. Jiang, Z., Huang, C. B., Leaird, D. E. & Weiner, A. M. Optical arbitrary waveform processing of more than 100 spectral comb lines. *Nature Photon.* **1,** 463–467 (2007).
13. Ferdous, F. *et al.* Spectral line-by-line pulse shaping of an on-chip microresonator frequency comb. *Nature Photon.* **5,** 770–776 (2011).
14. Savchenkov, A. A. *et al.* Tunable optical frequency comb with a crystalline whispering gallery mode resonator. *Phys. Rev. Lett.* **101,** 093902 (2008).
15. Grudinin, I. S., Yu, N. & Maleki, L. Generation of optical frequency combs with a CaF_2 resonator. *Opt. Lett.* **34,** 878–880 (2009).
16. Herr, T. *et al.* in *Proc. Quantum Electronics and Laser Science Conference* paper QTuF1 (Optical Society of America, 2011).
17. Liang, W. *et al.* Generation of near-infrared frequency combs from a MgF_2 whispering gallery mode resonator. *Opt. Lett.* **36,** 2290–2292 (2011).
18. Wang, C. Y. *et al.* Mid-infrared optical frequency combs based on crystalline microresonators. Preprint at http://arXiv.org/abs/1109.2716 (2011).
19. Agha, I. H., Okawachi, Y., Foster, M. A., Sharping, J. E. & Gaeta, A. L. Four-wave-mixing parametric oscillations in dispersion-compensated high-Q silica microspheres. *Phys. Rev. A* **76,** 043837 (2007).
20. Razzari, L. *et al.* CMOS-compatible integrated optical hyper-parametric oscillator. *Nature Photon.* **4,** 41–45 (2010).
21. Levy, J. S. *et al.* CMOS-compatible multiple-wavelength oscillator for on-chip optical interconnects. *Nature Photon.* **4,** 37–40 (2010).
22. Foster, M. A. *et al.* Silicon-based monolithic optical frequency comb source. *Opt. Express* **19,** 14233–14239 (2011).
23. Braje, D., Hollberg, L. & Diddams, S. Brillouin-enhanced hyperparametric generation of an optical frequency comb in a monolithic highly nonlinear fiber cavity pumped by a CW laser. *Phys. Rev. Lett.* **102,** 193902 (2009).
24. Del'Haye, P., Arcizet, O., Schliesser, A., Holzwarth, R. & Kippenberg, T. J. Full stabilization of a microresonator-based optical frequency comb. *Phys. Rev. Lett.* **101,** 053903 (2008).
25. Del'Haye, P. *et al.* Octave spanning tunable frequency comb from a microresonator. *Phys. Rev. Lett.* **107,** 063901 (2011).
26. Okawachi, Y. *et al.* Octave-spanning frequency comb generation in a silicon nitride chip. *Opt. Lett.* **36,** 3398–3400 (2011).
27. Savchenkov, A. A. *et al.* Kerr combs with selectable central frequency. *Nature Photon.* **5,** 293–296 (2011).

28. Chembo, Y. K., Strekalov, D. V. & Yu, N. Spectrum and dynamics of optical frequency combs generated with monolithic whispering gallery mode resonators. *Phys. Rev. Lett.* **104,** 103902 (2010).
29. Chembo, Y. K. & Yu, N. Modal expansion approach to optical frequency combs generation with monolithic whispering gallery mode resonators. *Phys. Rev. A* **82,** 033801 (2010).
30. Papp, S. B. & Diddams, S. A. Spectral and temporal characterization of a fused-quartz-microresonator optical frequency comb. *Phys. Rev. A* **84,** 053833 (2011).
31. Carmon, T., Yang, L. & Vahala, K. J. Dynamical thermal behavior and thermal self-stability of microcavities. *Opt. Express* **12,** 4742–4750 (2004).
32. Kippenberg, T. J., Spillane, S. M. & Vahala, K. J. Kerr-nonlinearity optical parametric oscillation in an ultrahigh-Q toroid microcavity. *Phys. Rev. Lett.* **93,** 083904 (2004).
33. Braginsky, V. B., Gorodetsky, M. L. & Vyatchanin, S. P. Thermodynamical fluctuations and photo-thermal shot noise in gravitational wave antennae. *Phys. Lett. A* **264,** 1–10 (1999).
34. Gorodetsky, M. L. & Grudinin, I. S. Fundamental thermal fluctuations in microspheres. *J. Opt. Soc. Am. B* **21,** 697–705 (2004).
35. Matsko, A. B., Savchenkov, A. A., Yu, N. & Maleki, L. Whispering-gallery-mode resonators as frequency references. i. fundamental limitations. *J. Opt. Soc. Am. B* **24,** 1324–1335 (2007).
36. Rokhsari, H., Kippenberg, T. J., Carmon, T. & Vahala, K. J. Radiation-pressure-driven micro-mechanical oscillator. *Opt. Express* **13,** 5293–5301 (2005).
37. Ma, R. *et al.* Radiation-pressure-driven vibrational modes in ultrahigh-Q silica microspheres. *Opt. Lett.* **32,** 2200–2202 (2007).
38. Savchenkov, A. A., Matsko, A. B., Ilchenko, V. S., Seidel, D. & Maleki, L. Surface acoustic wave opto-mechanical oscillator and frequency comb generator. *Opt. Lett.* **36,** 3338–3340 (2011).
39. Fomin, A. E., Gorodetsky, M. L., Grudinin, I. S. & Ilchenko, V. S. Nonstationary nonlinear effects in optical microspheres. *J. Opt. Soc. Am. B* **22,** 459–465 (2005).
40. Del'Haye, P., Arcizet, O., Gorodetsky, M. L., Holzwarth, R. & Kippenberg, T. J. Frequency comb assisted diode laser spectroscopy for measurement of microcavity dispersion. *Nature Photon.* **3,** 529–533 (2009).
41. Hofer, J., Schliesser, A. & Kippenberg, T. J. Cavity optomechanics with ultrahigh-Q crystalline microresonators. *Phys. Rev. A* **82,** 031804 (2010).
42. Bahl, G., Zehnpfennig, J., Tomes, M. & Carmon, T. Stimulated optomechanical excitation of surface acoustic waves in a microdevice. *Nature Commun.* **2,** 403 (2011).
43. Carmon, T., Cross, M. C. & Vahala, K. J. Chaotic quivering of micron-scaled on-chip resonators excited by centrifugal optical pressure. *Phys. Rev. Lett.* **98,** 167203 (2007).
44. Savchenkov, A. A., Rubiola, E., Matsko, A. B., Ilchenko, V. S. & Maleki, L. Phase noise of whispering gallery photonic hyper-parametric microwave oscillators. *Opt. Express* **16,** 4130–4144 (2008).
45. Agha, I. H., Okawachi, Y. & Gaeta, A. L. Theoretical and experimental investigation of broadband cascaded four-wave mixing in high-Q microspheres. *Opt. Express* **17,** 16209–16215 (2009).
46. Arcizet, O., Schliesser, A., Del'Haye, P., Holzwarth, R. & Kippenberg, T. J. in *Practical Applications of Microresonators in Optics and Photonics*, Ch. 11, 483–506 (CRC Press, 2009).
47. Matsko, A. B., Savchenkov, A. A., Strelakov, D., Ilchenko, V. S. & Maleki, L. Optical hyperparametric oscillations in a whispering-gallery-mode resonator: threshold and phase diffusion. *Phys. Rev. A* **71,** 033804 (2005).
48. Liang, W. *et al.* Whispering-gallery-mode-resonator-based ultranarrow linewidth external-cavity semiconductor laser. *Opt. Lett.* **35,** 2822–2824 (2010).
49. Carmon, T. *et al.* Static envelope patterns in composite resonances generated by level crossing in optical toroidal microcavities. *Phys. Rev. Lett.* **100,** 103905 (2008).
50. Matsko, A. B. *et al.* Optical Kerr frequency comb generation in overmoded resonators. Preprint at http://ArXiv.org/abs/1201.1959 (2012).

Author contributions
T.H. and T.J.K designed the experiments. T.H. and J.R. performed the experiments. T.H. analysed the data. K.H. fabricated the Si_3N_4 samples. E.G. contributed in the early phase of the Si_3N_4 sample fabrication. T.H. and C.Y.W. fabricated the MgF_2 samples. M.L.G., T.H. and T.J.K. developed the quantitative model. All authors discussed the data and wrote the manuscript.

Additional information
The authors declare no competing financial interests. Supplementary information accompanies this paper at www.nature.com/naturephotonics. Reprints and permission information is available online at http://www.nature.com/reprints. Correspondence and requests for materials should be addressed to T.J.K.